Optics Letters

Scaled model guidelines for solar coronagraphs' external occulters with an optimized shape

Federico Landini,[1,*] Cristian Baccani,[2] Hagen Schweitzer,[3] Daniel Asoubar,[3] Marco Romoli,[2] Matteo Taccola,[4] Mauro Focardi,[1] Maurizio Pancrazzi,[2] and Silvano Fineschi[5]

[1]INAF—Osservatorio Astrofisico di Arcetri, Largo E. Fermi 5, 50125 Firenze, Italy
[2]Università degli Studi di Firenze—Dipartimento di Fisica e Astronomia, Via Sansone 1, 50019 Sesto Fiorentino (Firenze), Italy
[3]LightTrans International UG, Kahlaische Straße 4, 07745 Jena, Germany
[4]ESA/ESTEC—Keplerlaan 1, NL-2200 AG Noordwijk ZH, The Netherlands
[5]INAF—Osservatorio Astrofisico di Torino, Via Osservatorio 20, 10025 Pino Torinese, Italy
*Corresponding author: flandini@arcetri.astro.it

Received 6 June 2017; revised 3 August 2017; accepted 23 October 2017; posted 23 October 2017 (Doc. ID 297469); published 17 November 2017

One of the major challenges faced by externally occulted solar coronagraphs is the suppression of the light diffracted by the occulter edge. It is a contribution to the stray light that overwhelms the coronal signal on the focal plane and must be reduced by modifying the geometrical shape of the occulter. There is a rich literature, mostly experimental, on the appropriate choice of the most suitable shape. The problem arises when huge coronagraphs, such as those in formation flight, shall be tested in a laboratory. A recent contribution [Opt. Lett. 41, 757 (2016)] provides the guidelines for scaling the geometry and replicate in the laboratory the flight diffraction pattern as produced by the whole solar disk and a flight occulter but leaves the conclusion on the occulter scale law somehow unjustified. This paper provides the numerical support for validating that conclusion and presents the first-ever simulation of the diffraction behind an occulter with an optimized shape along the optical axis with the solar disk as a source. This paper, together with Opt. Lett. 41, 757 (2016), aims at constituting a complete guide for scaling the coronagraphs' geometry.

OCIS codes: (260.1960) Diffraction theory; (350.1260) Astronomical optics; (220.4830) Systems design.

https://doi.org/10.1364/OL.42.004800

The very first experiment of observation of the visible solar corona with an externally occulted coronagraph was performed by Newkirk and Eddy in 1962 [1] with a stratospheric balloon and with little success. They used a simple knife-edge disk as an occulter, and the stray light due to diffraction off the occulter edge dominated the detected signal. The debate on the best optimizing solution to reduce the diffraction produced by the occulter has been ongoing since then. There is not an answer that satisfies every case: each solution shall fit the constraint of the mission and must have a minimum impact on the scientific objectives. There are two main optimization classes, based on different diffraction reduction strategies: scattering and occultation. The scattering-based optimization was first proposed by Purcell and Koomen in 1962 [2] and consists of a sharp single disk with a serrated edge. The case has been theoretically analyzed by Lenskii [3] and Aime [4] and experimentally tested by Fort et al. [5], Koutchmy [6], and Landini et al. [7]. A series of very tiny and sharp teeth is designed to spread diffracted light along the edge of the shadow of the disk itself in order to escape the pupil. The occultation-based optimization was first proposed and tested by Newkirk and Bohlin in 1963 [8] as a second, successful, attempt of the first balloon flight. The base version of this optimization consists of a second disk in the shadow of the first with respect to the solar disk light, with the role of blocking part of the light diffracted by the first disk edge. The stray light reduction performance was improved by adding further disks with the same principle. By increasing to several disks over a limited length along the optical axis, we end up in a multi-threaded frustum of a right cone. By pushing the disk number to the upper limit of infinity, the resulting occulter is a polished frustum of a right cone. Despite that this class of occultation is experimentally proven to be the most effective in reducing the stray light in most cases (see, for instance, [7,9,10]), it lacks a proper theoretical analysis. Lenskii only [3] performed a theoretical evaluation of the stray light on a single image point on axis behind a two-disk system. A proper simulation is so far lacking of the light diffracted by an occulter with an optimized geometrical shape along the optical axis.

The coming frontier in coronal imaging is formation flight (FF). By greatly increasing the distance between the occulter and the rest of the telescope, FF coronagraphs reduce the level of stray light generated by the occulter at fixed minimum field of view. PROBA-3ASPIICS [11,12] (Association of Spacecraft for Polarimetric and Imaging Investigation of the Corona of the Sun) and HiRISE [13] (High Resolution Imaging and Spectroscopy Explorer) are two examples. FF coronagraphs are characterized by occulters with diameters of the order of meters and occulter–pupil distances of the order of hundreds of meters. Such configurations make the indoor experimental

evaluation of the light diffracted by the occulter really challenging. A scaled model is mandatory, and a recent work [14] defines the scale law for a solar coronagraph in FF:

- Occulter dimension scaled by a factor f perpendicularly to the optical axis.
- Distance between the occulter and the entrance aperture scaled by a factor f^2 along the optical axis.
- Tangent of the solar divergence scaled by a factor $1/f$.
- Solar irradiance scaled by a factor f^2. Irrelevant in the case in which experimental activity is performed by normalizing the diffraction to the mean source brightness.

The scale law for an occulter with an optimized shape along the optical axis is only logically justified in [14], a demonstration not being provided: the occulter geometry shall be scaled by a factor f perpendicularly to the optical axis and by a factor f^2 along the optical axis. This paper aims at completing the set of rules provided by [14] by validating the proposed scale law.

In principle, two possible approaches can be pursued in order to validate the scale law:

- Experimental approach: at least two scaled models shall be manufactured with different scale factors, and the diffraction patterns at the corresponding scaled distances shall be compared.
- Numerical approach: simulations shall be performed with different scale factors and the resulting patterns compared.

In both cases, the diffraction patterns that are compared must be equal for the validation to be accomplished.

The experimental approach requires large time ranges to be allocated for the setup design and the tests, and it can eventually fail due to unpredicted practical hindrances, which often occur in laboratory activities. Nevertheless, it has hitherto been the only accessible path to the validation of the scale law, due to the difficulties in performing simulations of optimized occulters. This work, by presenting the first simulation of the diffraction behind an occulter with a shape optimized along the optical axis, validates the scale law suggested by [14] and constitutes a sound base for future experimental activities on the same subject.

In the following, first a description is given of the theory at the basis of the software that has been used, then the simulation parameters are defined, and finally, the results are presented.

For a numerical validation of the scale law, several field-tracing-based [15] simulations have been performed. A frustum of a right cone has been considered as a reference occulter shape for the whole set of simulations. The truncated cone is simulated by means of a series of N disks over a finite length L (see figure 1). The envelope defined by the disk edge draws the truncated cone surface. $\alpha_\odot$ is the solar disk divergence; all the External Occulter (EO) diaphragms shall lay in the shadow of the first diaphragm edge with respect to the marginal ray from the solar disk. In order to select the appropriate number of disks to emulate a conical surface, several diffraction simulations have been performed by changing the disk number. Figure 2 summarizes the analysis. The left y axis accounts for the ratio of the diffraction level on axis for the case of N disks with respect to the case of two disks as a function of N. As expected, the diffraction level behind the occulter decreases by increasing N, virtually matching the horizontal asymptote for $N = \infty$, i.e., the actual conical surface. The right y axis accounts for the percent deviation of the diffraction on axis for a N-disks occulter from the diffraction generated on axis by an ideal conical surface (please note that the axis scale is reversed to facilitate the graph readability). The deviation starts decreasing below 1% for $N \geq 15$. Thus, for the particular coronagraph geometry treated in this paper, we choose $N = 15$.

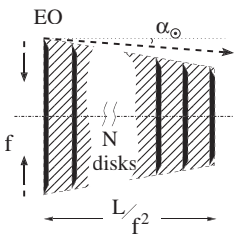

Fig. 1. Representation of a truncated cone as implemented in the simulations. N disks over a finite length have been used.

The optics design software VirtualLab Fusion [16] has been used to calculate the diffraction pattern that is generated by the occulter. For a realistic calculation of the light pattern behind the occulter, its depth as well as the lateral extension and the wavelength spectrum of the solar photosphere must be included in the simulations. The solar disk can be simulated by a set of incoherent point sources distributed all over its surface. Each source point generates a plane wave that impinges on the occulter. The radiation that impinges on the occulter can be described as a set of plane waves,

$$u^{\text{in}}_{a,b}(\boldsymbol{r}, t) = \sqrt{S(\lambda_b)}\, \exp\left[i\left(\boldsymbol{k}_{a,b} \cdot \boldsymbol{r} + \frac{2\pi c}{\lambda_b} t\right)\right], \quad \textbf{(1)}$$

with $u^{\text{in}}_{a,b}(\boldsymbol{r})$ representing the field of a single plane wave. λ_b represents a single wavelength of the photosphere's spectrum $S(\lambda)$. c is the speed of light. The sampling of the spectrum is denoted by $b = 1, 2, \ldots, P$; actually, for the sake of simplicity and in order to prove a principle, the diffraction simulations were performed at a fixed wavelength, but we prefer here to discuss the software theory at a more general level, as simplifications are always possible. The incident directions $a = 1, 2, \ldots, M$ of the plane waves are accounted for by the wave vectors $\boldsymbol{k}_{a,b} = (k_b \sin\vartheta_a \cos\varphi_a, k_b \cos\vartheta_a, k_b \sin\vartheta_a \sin\varphi_a) = (k_{x0,a}, k_{y0,a}, \sqrt{k_b^2 - k_{x0,a}^2 - k_{y0,a}^2})^T$ and the wavenumbers

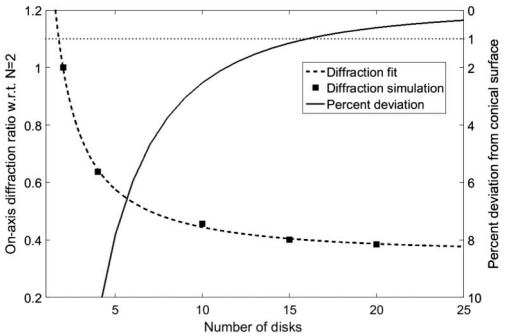

Fig. 2. Left y axis: ratio between the diffraction on axis behind an N-disks occulter and a two-disks occulter. Right y axis: percent deviation from the diffraction generated on axis by an ideal conical surface.

$k_b = 2\pi/\lambda_b$. The incident directions are denoted by the spherical coordinates ϑ_a and φ_a. $\boldsymbol{r} = (x, y, z)^T$ and t represent the position vector and the time, respectively. T denotes a transpose operator. For the calculation of the diffraction pattern $u_{a,b}^{\text{out}}$ per incident plane wave, the split-step beam propagation method (BPM) of VirtualLab Fusion is applied [17]:

$$u_{a,b}^{\text{out}}(z_0 + L/f^2) = \prod_{s=0}^{N-1}[\mathcal{P}_s(\Delta z)\mathcal{C}_s(z_0 + s\Delta z)]u_{a,b}^{\text{in}}(z_0), \quad (2)$$

with the number of BPM steps $N = L/(f^2\Delta z)$. Here $u_{a,b}^{\text{out}}(x, y, z_0 + L/f^2, t)$ is the diffraction pattern on an image plane behind the occulter, L/f^2 represents the total propagation distance, and Δz a single split-step distance. The split-step beam propagation method models the light propagation through an inhomogeneous region of an optical system by decomposing the inhomogeneity into N thin slices of length Δz. The light propagation through a single slice is performed with a two-step process. These are a diffraction-based free-space propagation step $\mathcal{P}_s(\Delta z)$ and a geometrical-optics-based light absorption as well as an optical path length change $\mathcal{C}_s(z_0 + s\Delta z)$. These two steps enable a modeling of diffraction and absorption by the occulter. The propagation starts with a single incident plane wave, applies the light absorption of the first slice, and performs a diffraction free-space propagation. The resulting field distribution at the end of slice one is used as a starting point for the propagation through slices two and so on. Since the occulter is a continuous 3D structure, it is required to decompose this region into a sufficiently large number of slices. The numerical conversions of the simulation results, depending on the number of slices, must always be checked (see Fig. 2). Since there is in this application only light absorption and diffraction within a slice and no optical path length change, this split-step beam propagation model can also be understood as a sequence of absorbing optical disks separated by thin free spaces (see Fig. 1). Please note that the (x, y, t) variable dependency of the field was skipped only for better readability. P_s is the angular spectrum of the plane waves operator [18], given by

$$\mathcal{P}_s u_{a,b}(z_0 + (s+1)\Delta z) = \mathcal{F}^{-1}\left\{\mathcal{F}[u_{a,b}(z_0 + s\Delta z)]\exp[\mathrm{i}\sqrt{k_b^2 - k_{x0,a}^2 - k_{y0,a}^2}\Delta z]\right\}. \quad (3)$$

Here $\mathcal{F}$ is the Fourier transformation with the conjugate variables $\boldsymbol{\rho} = (x, y)^T$ and $\boldsymbol{\kappa} = (k_x, k_y)^T$. Eq. (3) can be solved numerically efficiently using fast Fourier transformations (FFT). In $\mathcal{C}_s$, the light absorption at the truncated cone surface can be included as follows:

$$\mathcal{C}_s u_{a,b}(z_0 + (s+1)\Delta z) = \begin{cases} u_{a,b}(z_0 + s\Delta z) & \text{if } \sqrt{x^2 + y^2} > D/2 \\ 0 & \text{else} \end{cases}, \quad (4)$$

where D represents the diameter of the disk at the axial position $z_0 + s\Delta z$. The overall intensity distribution behind the occulter can be obtained by the incoherent summation over all fields,

$$I(x, y, z_0 + L/f^2) = \frac{\epsilon_0 c}{2}\sum_{a,b}(|u_{a,b}^{\text{out}}(x, y, z_0 + L/f^2)|^2), \quad (5)$$

with the vacuum permittivity ϵ_0.

Eventually, the resulting distribution is propagated down to the image plane by means of the above given angular spectrum of the plane waves operator (Eq. 3).

Diffraction simulations were performed in the following four cases (z indicates the occulter-image plane distance):

- Knife-edge disk. Occulter diameter 20 mm, $z = 1000$ mm. Solar disk at 1 AU (semidivergence ~0.267 degrees).
- Truncated cone, diameter 20 mm, $z = 1000$ mm (scale 1). Solar disk semidivergence ~0.267 degrees (1 AU).
- Truncated cone, diameter 2 mm, $z = 10$ mm (scale 10). Solar disk semidivergence ~2.67 degrees (0.1 AU).
- Truncated cone, diameter 200 mm, $z = 100$ m (scale 0.1). Solar disk semidivergence ~2.67×10^{-2} degrees (10 AU).

A dedicated discussion is required by the sampling definition. We can limit our scheme to a plane that contains the optical axis and is perpendicular to the occulter plane. From a computational point of view, the occulter is discretized, which allows us to imagine the occulter plane (on which the solar disk waves are impinging) as a diffraction grating and draw a parallel between the grating pitch and the sampling. Figure 3 sketches the described configuration. The goal is to get the first order of diffraction up to the extreme corner of the image plane. Each point of the finite diffraction grating shall be able to generate constructive interference on the whole image plane, up to the farthest corner. The diffraction grating has a finite dimension D_0, while the dimension of the image plane is $2R$. According to the grating equation at the first order, the following law shall be valid:

$$d = \frac{\lambda_b}{\sin\beta} = \frac{\lambda_b}{\sin\left[\arctan\left(\frac{D_0/2+R}{z}\right)\right]}, \quad (6)$$

where λ_b is a single wavelength, z is the distance between the occulter and the image plane, and d is the required sampling. According to the Nyquist–Shannon sampling theorem [19], the required sampling on the image plane should be at least $d/2$.

As anticipated, the solar disk extension has been simulated by means of a square grid of point sources. The points whose coordinates exceed the solar disk surface have been discarded. The sampling of the solar disk has an impact on the diffraction curves' modulation and on the computing time. As a trade-off

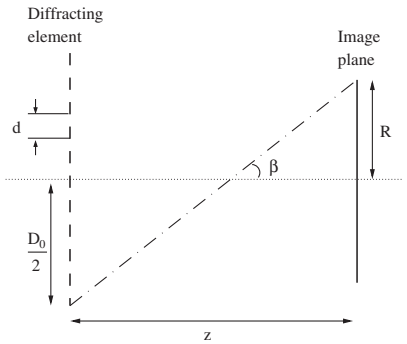

Fig. 3. Geometry for the parallel between the grating theory and the sampling definition.

Table 1. Sampling Parameters for the Simulations

	Sampling (μm)	
Simulation type	**Impinging wave**	**Image plane**
Knife edge	10	5
Cone, scale 1	10	5
Cone, scale 10	1	0.5
Cone, scale 0.1	100	50

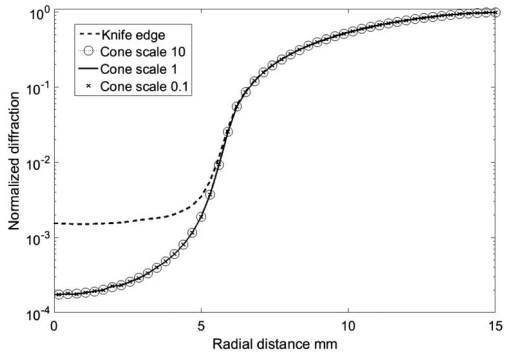

Fig. 4. Comparison between the knife-edge occulter and the truncated cones.

between the calculation time and the smoothness of the curves, 121 points have been chosen for the knife-edge case and 81 points for the truncated cones. Table 1 summarizes the sampling parameters that have been used for the calculation. Figure 4 shows the results of the comparison among the knife edge and the truncated cones. For better readability, a subset of diffraction points has been interpolated from the resulting simulation pattern. It is worth pointing out that this is the first simulated comparison of the performance of a truncated cone with respect to a knife-edge occulter. The performance improvement is confirmed as described in the experimental literature. The truncated cone curves are overlapped; in order to emphasize the discrepancies among the truncated cone curves at different scales, the percent differences with respect to the scale 1 case are shown in Fig. 5 for an x range limited to the portion of the whole pattern where the largest discrepancies are observed. Again, in order to appreciate the curves' behavior in detail, only a selection of the available points are presented. There is a slight fluctuation that is due partially to the impinging wave sampling, which is at the upper limit

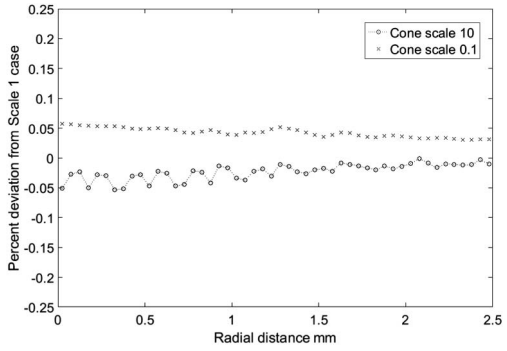

Fig. 5. Percent difference of the diffraction behind scaled truncated cones with respect to the scale 1 case.

of the value defined by Eq. (6) and partially to the solar disk sampling. The approximation of the proposed scale law [14] is correct within 0.1%, which is well below the typical measurement errors of diffraction laboratory tests [7,20].

In summary, taking advantage of the first diffraction simulation behind a solar coronagraph occulter optimized along the optical axis, we verified the method proposed in [14] for longitudinally scaling the occulter dimension. The verification was performed by comparing the diffraction pattern behind a conical occulter in three different scale cases. The method has an intrinsic approximation due to the second-order truncation of the Fresnel–Kirchhoff diffraction integral, but the uncertainty is within the typical experimental tolerances of diffraction measurements.

As a completion of the discussion begun in [14] and in order to provide an operational guide to manufacture a f-scaled model of an externally occulted solar coronagraph, the scale law can be summarized as follows:

- As for the coronagraph geometry, all dimensions perpendicular to the optical axis shall be scaled by a factor f. All dimensions along the optical axis (optimized occulter shape included) shall be scaled by a factor f^2.
- As for the source, the tangent of the solar angular divergence shall be scaled by a factor $1/f$, and the solar irradiance shall be scaled by a factor f^2.

These scale guidelines are going to be experimentally verified soon in the case of the PROBA3/ASPIICS coronagraph during the measurement campaign that is currently being set up [21].

REFERENCES

1. G. Newkirk, Jr. and J. A. Eddy, S&T **24**, 77 (1962).
2. J. D. Purcell and M. J. Koomen, J. Opt. Soc. Am. **52**, 596 (1962).
3. A. V. Lenskii, Sov. Astron. **25**, 366 (1981).
4. C. Aime, Astron. Astrophys. **558**, A138 (2013).
5. B. Fort, C. Morel, and G. Spaak, Astron. Astrophys. **63**, 243 (1978).
6. S. Koutchmy, Space Sci. Rev. **47**, 95 (1988).
7. F. Landini, M. Romoli, G. Capobianco, S. Vives, S. Fineschi, G. Massone, D. Loreggia, E. Turchi, C. Guillon, C. Escolle, M. Pancrazzi, and M. Focardi, Proc. SPIE **8862**, 886204 (2013).
8. G. Newkirk, Jr. and D. Bohlin, Appl. Opt. **2**, 131 (1963).
9. S. Koutchmy and M. Belmahdi, J. Opt. **18**, 265 (1987).
10. M. Bout, P. Lamy, A. Maucherat, C. Colin, and A. Llebaria, Appl. Opt. **39**, 3955 (2000).
11. S. Vives, P. Lamy, F. Auchere, J.-C. Vial, S. Koutchmy, J. Arnaud, J.-Y. Prado, F. Frassetto, and G. Naletto, Proc. SPIE **5901**, 305 (2005).
12. P. Lamy, L. Damé, S. Vivès, and A. Zhukov, Proc. SPIE **7731**, 773118 (2010).
13. L. Damé, *Proceedings of the 2nd Symposium IAGA* (2010).
14. F. Landini, M. Romoli, C. Baccani, M. Focardi, M. Pancrazzi, D. Galano, and V. Kirschner, Opt. Lett. **41**, 757 (2016).
15. F. Wyrowski and M. Kuhn, J. Mod. Opt. **58**, 449 (2011).
16. Lighttrans, http://www.lighttrans.com (2017).
17. M. D. Feit and J. A. Fleck, Appl. Opt. **17**, 3990 (1978).
18. L. Mandel and E. Wolf, *Optical Coherence and Quantum Optics* (Cambridge University, 1995).
19. J. W. Goodman, *Introduction to Fourier Optics* (McGraw Hill, 1996).
20. F. Landini, S. Vives, M. Venet, M. Romoli, C. Guillon, and S. Fineschi, Appl. Opt. **50**, 6632 (2011).
21. F. Landini, C. Baccani, S. Vives, S. Fineschi, M. Romoli, G. Capobianco, G. Massone, M. Casti, A. Bemporad, M. Focardi, M. Pancrazzi, D. Loreggia, V. Noce, A. Corso, C. Thizy, E. Renotte, and B. Marquet, Proc. SPIE **10397**, 103971C (2017).